20XX-01-XXXX

The Effect of Swirl on the Flow Uniformity in Automotive Exhaust Catalysts

Author, co-author (Do NOT enter this information. It will be pulled from participant tab in MyTechZone)

Affiliation (Do NOT enter this information. It will be pulled from participant tab in MyTechZone)

Abstract

In aftertreatment system design, flow uniformity is of paramount importance as it affects aftertreatment device conversion efficiency and durability. The major trend of downsizing engines using turbochargers means the effect of the turbine residual swirl on the flow needs to be considered. In this paper, this effect has been investigated experimentally and numerically. A swirling flow rig with a moving-block swirl generator was used to generate swirling flow in a sudden expansion diffuser with a wash-coated diesel oxidation catalyst (DOC) downstream. Hot-wire anemometry (HWA) was used to measure the axial and tangential velocities of the swirling flow upstream of the diffuser expansion and the axial velocity downstream the monolith. With no swirl, the flow in the catalyst monolith is highly non-uniform with maximum velocities near the diffuser axis. At high swirl levels, the flow is also highly non-uniform with the highest velocities near the diffuser wall. An intermediate swirl level exists where the flow is most uniform. To gain further insight into the mechanisms controlling flow redistribution, numerical simulations have been performed using the commercial CFD code STARCCM+. With no swirl, the central jet transverses the diffuser, and a drastic flow redistribution takes place near the monolith face due to its high resistance. Immediately downstream of the sudden expansion, the flow separates from the diffuser wall forming a separation zone around the central jet. Increasing swirl reduces the size of this separation zone, and eventually leads to the formation of the central recirculation zone characteristic of high swirl flows. At intermediate swirl levels, the size of the wall separation zone is reduced considerably, while the axial adverse pressure gradient is insufficient to cause a central recirculation. Such a flow regime occurs at relatively low swirl levels ($S \sim 0.23$). This may have positive implications for aftertreatment system design with low residual swirl levels from the turbine, which might be tuned by adjusting the distance between the turbine and the catalyst or employing guide vanes. The findings can be directly transferred to other aftertreatment systems with a catalyst or particulate filter. Moreover, swirling flows with an obstruction or a high resistance device downstream (e.g. a heat exchanger or filter) are present in many other applications such as cooling flows, combustion and turbomachinery. Therefore the results are relevant to a much wider research and industrial community.

Introduction

Catalytic converters are used in the automotive industry to comply with increasingly stringent emissions regulations. Automotive catalysts are monolith structures comprised of many parallel channels of small hydraulic diameter ~ 1mm. Precious metals are applied to the channel walls (as a thin washcoat) thus providing the high surface area on which exhaust constituents can react. Optimum performance requires that the residence time (or flow velocity) of the exhaust in the monolith is the same for all channels. Indeed, the degree of flow maldistribution across the monolith is often used as a criterion for assessing the acceptability of a particular design.

The size of the monolith is largely dictated by engine capacity and operating mode. Its length is normally kept as short as possible to reduce pressure loss. A typical cylindrical monolith for a passenger vehicle would have a diameter of around 100 mm and length around 150 mm. Space limitations often mean that short, wide-angled diffusers are used to join the exhaust pipe to the front face of the monolith. This results in flow separation within the diffuser and a non-uniform flow distribution within the monolith.

Figure 1 shows a schematic of the flow field in an axisymmetric catalyst assembly. Flow separates on entering the expander with the resulting jet traversing the diffuser before rapidly spreading a short distance upstream of the monolith. Part of the exhaust gas enters the monolith channels, while some of it reverses to feed the large recirculating vortices within the diffuser. The net result is that the flow entering the monolith is maldistributed with the central channels subject to higher velocity. Shorter residence time results in lower conversion efficiency and can lead to high thermal loading and premature deactivation [1]. Flow separation also produces higher system pressure loss and increased fuel consumption [2].

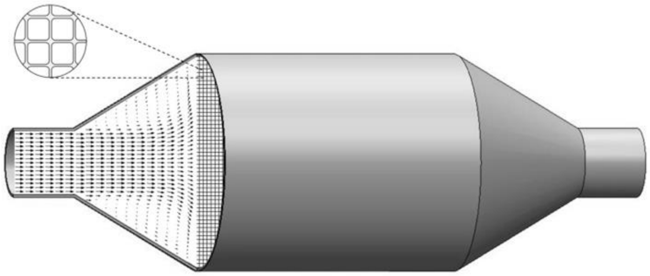

Figure 1. Schematic of the flow field in a catalyst assembly.

To improve thermal efficiency and reduce carbon emissions, automotive manufacturers are using downsized, turbo-charged engines. This will have a knock-on effect on after-treatment systems as the exhaust flow and temperature field will be modified by the presence of the turbo-charger. In particular, the flow exiting the turbocharger will have a significant swirl component depending on engine operating conditions and turbocharger characteristics. The effect of swirl on the flow field within the diffuser and the monolith is largely unknown.

In simpler geometries, such as straight pipes and diffusers with no flow restrictions downstream, the effect of swirl on the flow distribution has been the subject of much fundamental and applied research [3]-[10]. For wide-angle open diffusers, Okhio et al. [5] have shown that increasing swirl number can suppress separation - clearly of benefit for catalyst assemblies. However, high swirl can lead to the development of very low pressures in the centre of the vortex leading to flow reversal accompanied by a strong recirculating zone within the diffuser and additional pressure loss [5]-[8]. Very few studies exist of the effect of the downstream conditions on the flow structure. These usually involve a flow constriction at a considerable distance from the swirl generator which has been shown to have a strong influence on the entire flow field [9]. In contrast, the exhaust after-treatment assembly features a significant resistance, namely the monolith, in close proximity to the diffuser outlet. The authors are not aware of any flow studies which have been reported for these situations. This paper presents an experimental and numerical investigation of the flow distribution across an automotive monolith as a function of swirl ratio and mass flow rate.

Experimental Study

Experimental setup

A schematic of the swirling flow rig is shown in Figure 2. The rig features a swirl generator (2) - (4) placed upstream of an axisymmetric catalyst assembly (6) - (7). The swirl generator is based on the moving-block principle [12], a design that has been widely used in gas turbine research. Its main advantage is its compactness and the ability to easily adjust the swirl ratio.

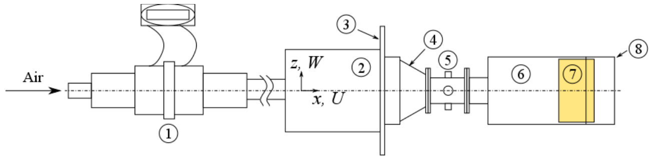

Figure 2. Schematic of the swirling flow rig used in the study.

Air from a compressor is supplied to the test rig, with the flow rate measured by a calibrated viscous flow meter (VFM) (1). Air enters the plenum (2) before passing through a set of movable blocks that can be positioned to generate varying levels of swirl by adjusting the moveable plate (3). Air then enters the co-axial nozzle (4) and a transparent annular extension piece (5). The transparent extension piece (55 mm inner diameter with a 24 mm diameter annular insert) provides access for the hot-wire anemometry (HWA) probe and a thermocouple used for measurement of the axial and tangential velocity components across the annulus. A sudden expansion diffuser (6) connects the swirl generator assembly to the monolith (7) of diameter, D = 145.8 mm, followed by an outlet sleeve (8).

The sudden expansion diffuser ((6) in Figure 2) features inlet and outlet diameters of 55 and 145.8 mm, respectively. A 50-mm-length, 55-mm-diameter inlet pipe connects the diffuser to the transparent extension piece (5) of the swirl generator. The monolith was fitted 162 mm downstream from the expansion and is a cordierite, wash-coated diesel oxidation catalyst (DOC) of 76.2-mm-length and 143.8-mm-diameter with a nominal cell density of 400 cpsi.

Velocities across the annular transparent extension piece at the outlet of the swirl generator as well as downstream of the monolith were measured using a TSI IFA 300 constant temperature HWA system with Dantec 55P11 single-normal (SN) HWA probes. Calibration of the probes was performed using an automatic TSI 1129 calibration rig with the probe stem and the hot wire both perpendicular to the flow direction.

Velocity measurements across the annular transparent extension piece were made with the HWA probe stem aligned with the y-axis (Figure 3). Sampling of the analogue HWA signal was made at 200 Hz for a duration of 5 s. The probes are calibrated to measure the velocity magnitude with the wire aligned perpendicular to the flow direction. In the current configuration, the flow direction in the annulus is not known a priori and varies with the probe y-position. Therefore, a methodology has been developed in order to align the probe with the mean flow vector at the various swirl intensities to obtain the velocity magnitude.

To measure the flow profile in the annular section, the HWA probe was traversed across the annulus radius at 1 mm intervals. At each traversed position the probe was rotated around its axis and the signal was recorded every 4° for 360° of total rotation. It was established that a 4° rotation interval was sufficient to determine the flow direction with required accuracy. The datum for the angular positioning of the HWA probe can be chosen arbitrarily but has to be set constant with respect to the rig geometry for all traversed positions.

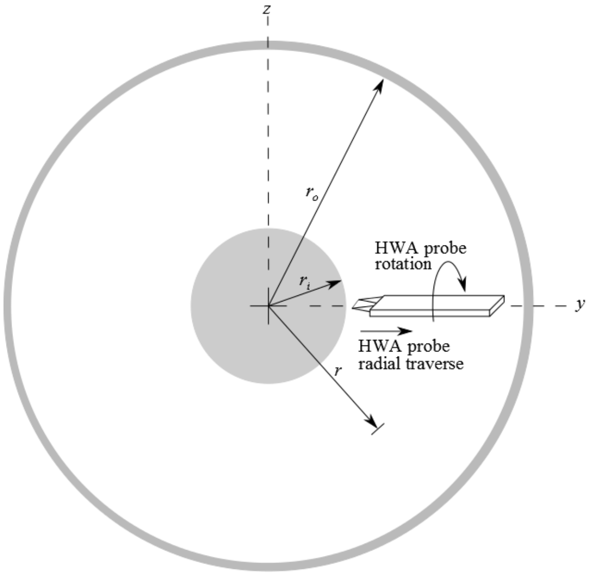

Figure 3. Schematic representation of HWA measurements made within the transparent annular extension.

A typical HWA response at one radial position is shown in Figure 4. The least squares method is used to obtain the voltage maxima and their angular positions. These correspond to the hot wire sensor being perpendicular to the flow, therefore velocity magnitude and flow direction can be obtained for each radial position inside the annulus.

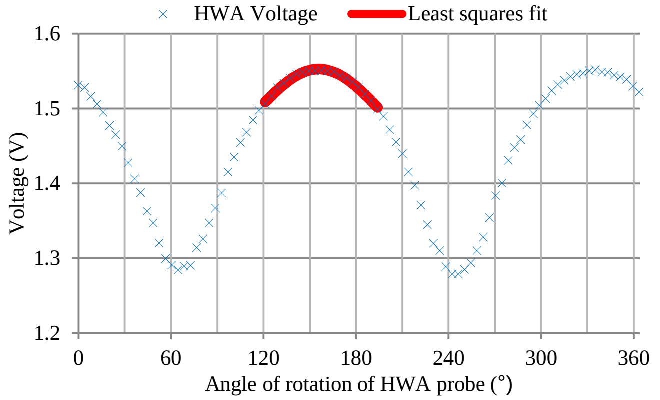

Figure 4. HWA output with varying angular positioning of the probe within the annular transparent extension.

The datum point for the HWA sensor (when it is orthogonal to the *x*-axis and lying in the *xz*-plane, see Figure 2) is determined by adopting the above methodology for zero swirl flow. For non-zero swirl flows, the angles obtained from the peaks of the HWA output were subtracted from the datum angle, thus obtaining the actual flow angle.

Positioning of the probe within the annular transparent extension was accomplished through a custom-built probe positioning mechanism (Figure 5). Radial positioning of the probe in the annular transparent extension piece was achieved using combinations of 1- and 2-mm aluminium spacers mounted along the probe support. Rotation of the probe around its axis was achieved using a stepper motor-pulley setup driven via an Arduino microcomputer interfaced to a custom-built LabVIEW GUI.

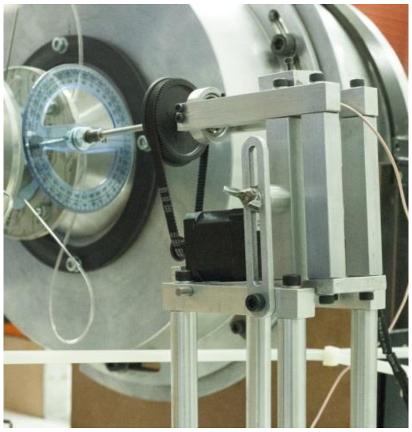

Figure 5. HWA probe positioning mechanism for angular and radial traverse of the HWA probe.

Velocity profiles downstream of the DOC were measured using a SN HWA probe with the probe stem aligned parallel to the mean flow direction. The probe was calibrated with the probe stem parallel to the axis of the calibration nozzle, and the analogue HWA signal was sampled at 1 kHz for a duration of 1 s. A two-axis programmable traverse system was used to traverse the HWA probe along the two diameters of the outlet sleeve (horizontal and vertical). Measurements were made 30 mm downstream of the monolith outlet. At this distance the jets exiting the monolith from adjacent channels will have mixed sufficiently to provide smooth radial profiles at the rear of the monolith.

Pressure tappings along the diffuser wall allowed measurement of the wall pressure distribution using water manometers. More tappings were used around the expansion point and just upstream of the DOC where the highest pressure variation was expected to occur.

Two mass flow rates were considered, 63 and 100 g/s, which are typical of 2.5-*l* engines operating at full load between 2500-4000 rpm at 100% volumetric efficiency. The swirl intensity was varied by adjusting the angle of the moveable plate of the swirl generator from 0° (no swirl) to 18° (high swirl).

Results

In order to characterise the level of swirl, a non-dimensional swirl number, S, can be defined as

$$S = \frac{G_\theta}{G_x r_o}, \tag{1}$$

where the swirl and axial momentum fluxes, G_θ and G_x, are given by

$$G_\theta = \int_{r_i}^{r_o} \rho U W r \, 2\pi r dr \tag{2}$$

$$G_x = \int_{r_i}^{r_o} \rho U^2 \, 2\pi r dr \tag{3}$$

In Eqs. (2) and (3), ρ is the air density, U is the axial velocity component, W is the tangential velocity component, and r is the radial distance from the centre of the annular cross-section of r_o and r_i outer and inner radii, respectively (Figure 3). The swirl number values estimated from the velocity measurements at the exit from swirl generator are shown in Table 1.

Figure 6 and Figure 7 show the axial and tangential velocity profiles in the annulus upstream of the expansion, normalised using the mean axial velocity. Here, the non-dimensionalised distance across the annulus is defined as $d = (r - r_i)/(r_o - r_i)$.

The velocity profiles at zero swirl and S = 0.23/0.26 are very similar for both mass flow rates, with some variation near the walls. At the higher swirl rates, the effects of swirl on the axial velocity profiles becomes more apparent. Velocities closer to the annulus inner wall are lower than those for no swirl and low swirl flow conditions. At the highest swirl level considered a significant amount of flow is directed towards the outer wall causing the axial velocities to peak at around d = 0.8 from the annulus inner wall.

The effect of swirl on the tangential velocity profiles is shown in Figure 7. At low swirl levels, the tangential velocity increases towards the outer wall of the annulus. As swirl is increased, the peak in the tangential velocity profile gradually gets closer to the inner wall of the annulus. At the highest swirl, where maximum velocities appear 1/3 of the way from the annulus inner wall, a typical Rankine vortex flow pattern is observed.

Changes in the mass flow rates do not appear to significantly affect the flow pattern for any of the swirl levels considered.

In order to check the accuracy of the flow measurements in the annulus, the air mass flow rate was calculated from the HWA axial velocity measurements. A good agreement with the mass flow rate measurements from the VFM was obtained, thus validating the methodology (Table 2).

Table 1. Estimated swirl number values

	Swirl number, ***S*** (experiments)		Swirl number, ***S*** (simulation)
Swirl generator angle	**63 g/s**	**100 g/s**	**63 g/s**
4° (low swirl)	0.23	0.26	0.25
7° (intermediate swirl)	0.44	0.45	0.47
10° (intermediate swirl)	0.70	0.63	0.69
18° (high swirl)	1.65	1.63	1.42

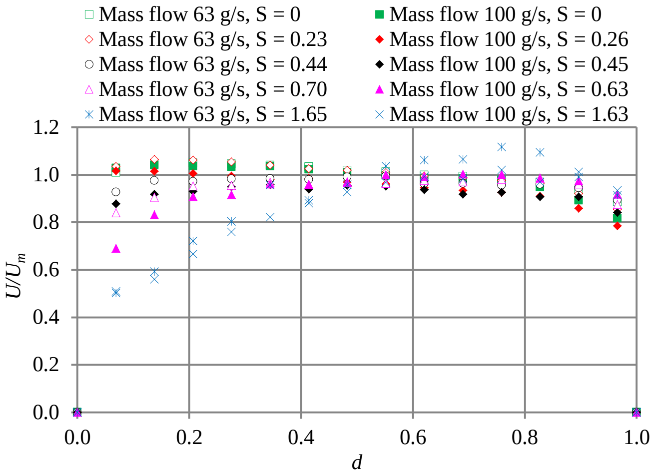

Figure 6. Normalised axial velocity profiles across annulus of swirl generator outlet. Filled and non-filled markers indicate measurements at 100 and 63 g/s, respectively.

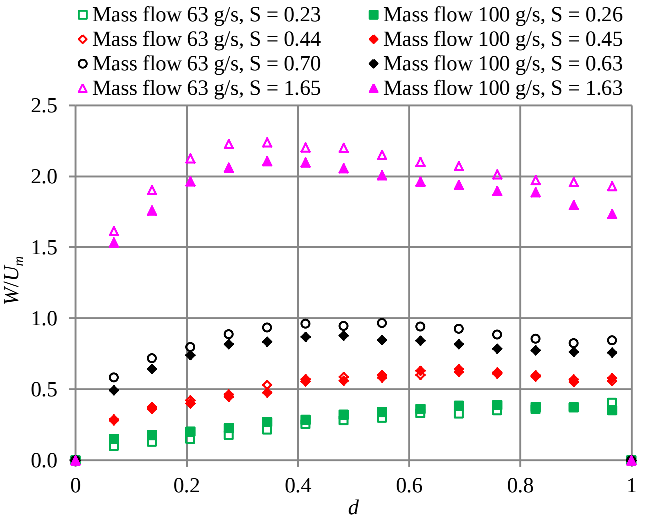

Figure 7. Normalised tangential velocity profiles across the annulus of the swirl generator outlet.

Table 2 The difference between mass flow rate measurements from VFM and calculated mass flow rates from HWA data. HWA1 refers to HWA measurements at the swirl generator exit, HWA2 refers to HWA measurements downstream of the catalyst.

Swirl generator angle	**Error (%) calculated using HWA1**		**Error (%) calculated using HWA2**	
	63 g/s	**100 g/s**	**63 g/s**	**100 g/s**
0° (no swirl)	-4.3	-6.4	-0.8	-4.6
4° (low swirl)	-4.8	-10.1	0.5	-2.5
7° (intermediate swirl)	-7.1	-11.2	-0.8	-1.2
10° (intermediate swirl)	-8.2	-8.0	7.4	3.5
18° (high swirl)	-8.8	-13.4	17.6	18.5

Figure 8 shows the velocity profiles measured along two diameters and demonstrates the flow is approximately axisymmetric in the monolith. As the flow was determined to be axisymmetric, the averages of the two traverse directions are presented in Figure 8 for all flow conditions.

With no swirl the velocity profiles exhibit a peak on the axis of the DOC where the jet from the inlet pipe enters the monolith. However, high resistance presented by the monolith causes the jet to spread outwards towards the diffuser outer wall. This causes the pressure to rise in the outermost regions of the diffuser wall forcing flow through this region resulting in the secondary peaks in the velocity profile.

At low swirl (swirl generator angle of 4°) the velocities are relatively flat for both mass flow rates. Due to radial pressure gradients induced by the swirling motion, more of the flow is directed towards the diffuser wall, resulting in higher velocities in the outer region of diffuser.

With further increase in swirl, the velocity magnitude near the wall continues to rise. At the intermediate swirl level (swirl generator angle of 7°) the normalised axial velocity near the wall is almost eight times higher than that in the centre. At the same time, an adverse axial pressure gradient starts to develop near the axis of the assembly causing a "dip" in the velocity profile.

At swirl generator angle of 10° and 18° the onset of reversed flow is observed in the centre of the diffuser. Note that hot wire anemometry only measures velocity magnitude, therefore the reverse flow appears as another peak at the centre of the diffuser. This is the reason for high mass flow rate calculation error (Table 2) for high swirl levels. The direction of the flow for 10° and 18° swirl generator angles was checked in a previous study using a shielded probe [13], and it was confirmed that the velocities in the middle of the diffuser were indeed negative.

The effect of the change in mass flow rate from 63 g/s to 100 g/s is insignificant, and the flow structure is clearly dominated by swirl.

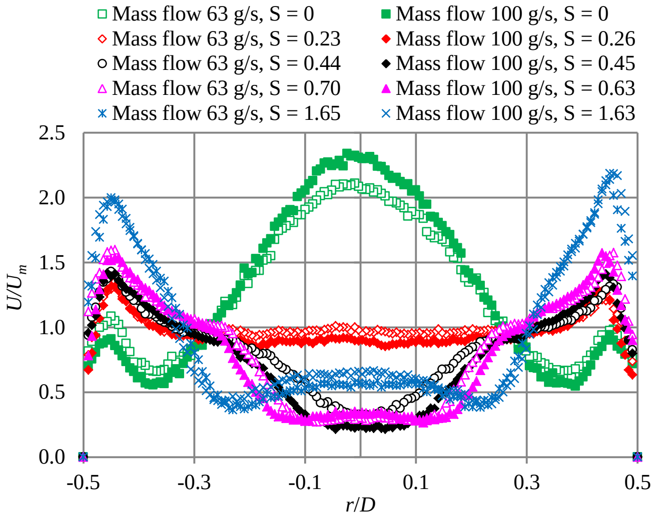

Figure 8. Normalised velocity profiles 30 mm downstream of the DOC where D is the diameter of the outlet sleeve and r is the distance from the axis.

Since flow uniformity is an important factor in catalyst design, it is instructive to introduce the flow maldistribution index, M, in the monolith [2]:

$$M = \frac{(\text{Peak velocity} - \text{Mean velocity})}{\text{Mean velocity}} \qquad (4)$$

In Eq. (4) the peak and mean velocities refer to the highest and average velocity magnitudes, respectively, obtained from HWA measurements across the outlet sleeve for any particular swirl number.

Table 3 shows the maldistribution index for all experimental conditions. Maldistribution is lowest at low swirl levels. For all swirl levels, the maldistribution increases with flow rate, a characteristic that has been reported previously in the literature [14, 15].

Another parameter used to assess flow uniformity is flow distribution index/flow uniformity index [16] defined as

$$\gamma = 1 - 0.5\frac{\sum \left| U_i - \bar{U} \right| A_i}{2\bar{U}A_{total}} \qquad (5)$$

where $\bar{U}$ is the mean velocity, U_i are measured velocities, A_i are corresponding annular segment areas and A_{total} is the total area of the annulus cross-section. The value of γ = 1 corresponds to fully uniform flow.

The flow uniformity index shown in Table 3 confirms the fact that low swirl level ($S \approx 0.23$) provides most uniform flow.

Table 3. Maldistribution index at different flow conditions.

Swirl generator angle	**Maldistribution index, *M***		**Flow uniformity index, γ**	
	63 g/s	**100 g/s**	**63 g/s**	**100 g/s**
0° (no swirl)	0.69	0.83	0.86	0.83
4° (low swirl)	0.40	0.48	0.96	0.94
7° (intermediate swirl)	0.76	1.02	0.91	0.88
10° (intermediate swirl)	1.13	1.29	0.87	0.85
18° (high swirl)	1.37	1.39	0.79	0.78

CFD Modelling

In order to gain insight into the flow structure within the diffuser CFD simulations have been performed for a mass flow rate of 63 g/s.

Model setup

The commercial CFD code StarCCM+ was used to model the flow. It is known that inlet conditions have a significant effect on the simulation results [17]. Therefore the full assembly together with swirl generator was considered. The geometry is shown in Figure 9. It includes the swirl generator (2-4 in Figure 2), extension piece (5 in Figure 2), diffuser (6 in Figure 2), monolith (7 in Figure 2) and the outlet sleeve (8 in Figure 2). As the swirl generator has 8 identical blocks spread azimuthally [10], a 45-degree wedge is used with periodic boundaries on each side.

A polyhedral mesh was used in all calculations. Ten prism layers were added at the walls, inlet and outlet boundaries in order to capture high gradients normal to these surfaces. Turbulence was modelled using the Reynolds-averaged Navier-Stokes (RANS) v^2f model, which is known to perform well in separating flows [18]. A two-layer low Reynolds number wall treatment was used with $y+ < 5$ in all simulations. A mesh independence study was performed for each swirl levels, resulting in five grids comprising 2 - 2.1M cells each. All simulations were performed using the SIMPLE algorithm. The equations were discretised using a second-order upwind scheme.

Uniform velocity, 1% turbulence intensity and turbulent viscosity ratio of 10 were specified at the swirl generator inlet. A constant pressure condition (p = 0) was used at the outlet. Periodic boundaries were specified at the side surfaces, and non-slip conditions were applied at the walls.

The flow in the monolith was modelled using a porous medium approach, where the monolith with parallel flow channels is modelled as a porous medium that resists the flow. Thus individual channels are not modelled which reduces meshing and computational time [19]. The resistance coefficients were estimated from experimental data obtained under cold flow conditions [13] using a correlation $\Delta p / L = \alpha u + \beta u|u|$. Here Δp is pressure drop, u is superficial velocity, L is the monolith length, α = 684.37 kg/m^{3}s and β = 28.28 kg/m^4 are viscous and inertial resistance coefficients, respectively. The resistance coefficients (both viscous and inertial) in the y and z directions were set to 10^5 to ensure that the flow in the monolith is unidirectional.

Additional resistance is introduced in the monolith due to the oblique entrance of the flow into the channels [20]. This was implemented in the model as a momentum source term $\Delta p_{oblique} = \pm \rho v^2/2$, where ρ is the air density and v is velocity tangential to the monolith front face at a distance 1 mm from the front face of the monolith. The sign is chosen so that the resultant force opposes the flow.

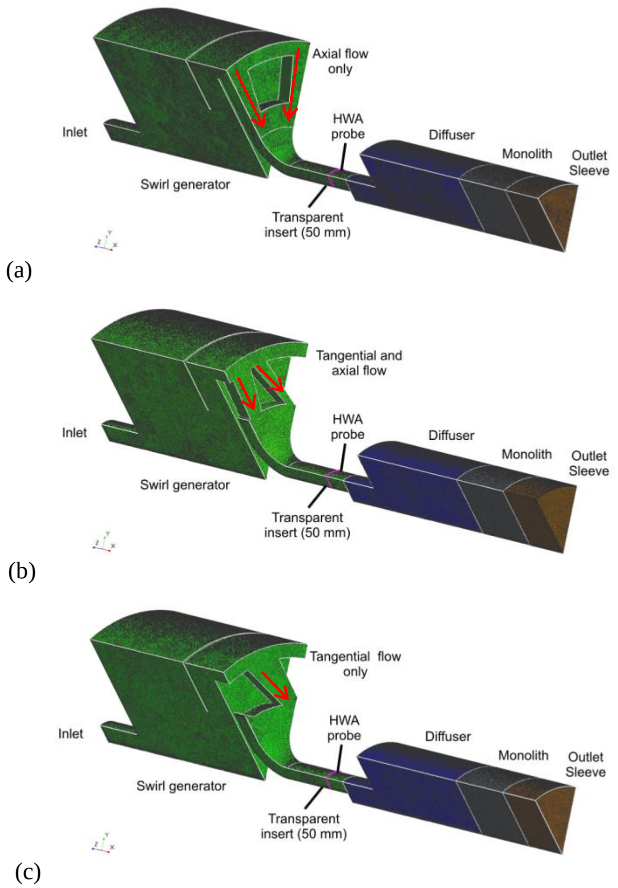

Figure 9. Geometry and mesh used in simulations: no swirl (a), 7° (b) and 18° (c) swirl generator angles.

Inlet conditions

Setting inlet conditions for swirling flows is a non-trivial task. Previous research has shown that in many swirling flow configurations the flow features are often closely coupled to and affect the flow upstream [17]. Therefore, prescribing the flow immediately upstream of the test section may cause unphysical flow behaviour, and also result in suppressing some of the flow features. This was observed in preliminary modelling in this study, and including the whole swirl generator assembly has been used to address this issue.

Comparison between simulation results and hot wire measurements at the outlet of the swirl generator (Figure 10 and Figure 11) shows a very good agreement in the axial velocities for all swirl levels. Tangential velocity distribution is not predicted as well (Figure 11). For the highest swirl (S = 1.65), simulation results show swirl levels characteristic to solid body rotation, while the experimental measurements have a swirling component maximum near the inner wall of the annular section. This could be a deficiency in the turbulence model which assumes isotropic turbulence even under swirling conditions.

The values of swirl number are shown in Table 1 and are in reasonable agreement with the experimental ones, apart from the highest swirl case where the swirl level is underpredicted upstream of the assembly as shown in Figure 11. The results show that CFD still captures most of the important features of the flow, which will be discussed below. Therefore, it can be argued that the level of swirl upstream is more important than the exact swirl velocity profile.

As shown previously, for all swirl levels the flow in the diffuser, monolith and outlet sleeve is nearly axisymmetric, therefore only one azimuthal cross-section is considered. For convenience, the values of swirl numbers calculated from the experiments will be used in discussing both experimental and simulation results.

No swirl (S = 0)

The flow structure and pressure distribution in the diffuser for $S = 0$ is shown in Figure 12. A small recirculation zone is formed behind the solid insert in the swirl generator outlet. A large recirculation zone is formed in the main body of the diffuser, away from the central jet. This separation zone extends along the whole side wall of the diffuser.

When the central annular jet reaches the monolith, high resistance of the monolith channels causes the flow to slow down, and the jet spreads towards the wall of the diffuser. Therefore there is dramatic flow redistribution just upstream of the monolith. A high pressure area is observed at the front face of the monolith where the flow decelerates. When the diverted flow reaches the wall, the pressure rises with some of the flow entering the monolith near the wall, and the remainder feeding the diffuser vortex. This causes a secondary axial velocity peak near the wall (Figure 13).

The pressure coefficient, c_p, is defined as

$$c_p = \frac{p - p_\infty}{0.5\rho U^2}\ , \qquad (6)$$

where ρ is air density, p is wall static pressure at the measurement location, p_∞ is the atmospheric pressure and U the average axial velocity in the annular section.

Pressure along the wall of the diffuser (Figure 14) is nearly constant, increasing just upstream of the monolith. A stagnation point is present at the diffuser wall where the separation zone ends, and a pressure maximum is observed. The trend in predicted pressure matches well with experiment.

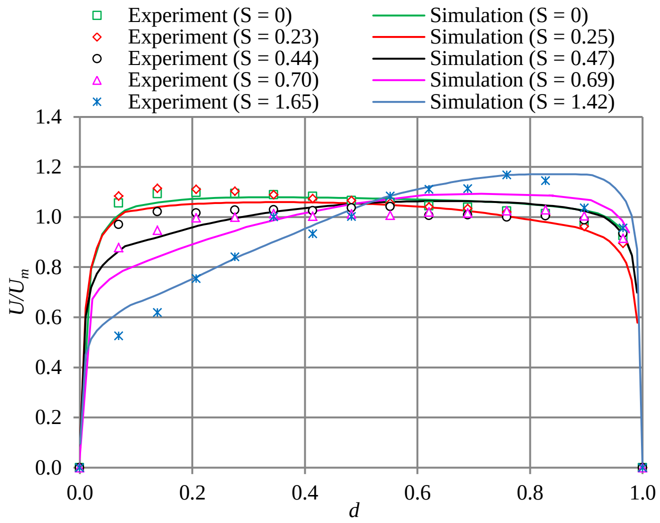

Figure 10. Normalised axial velocity: comparison between experiment and simulations for 63 g/s mass flow within the annulus.

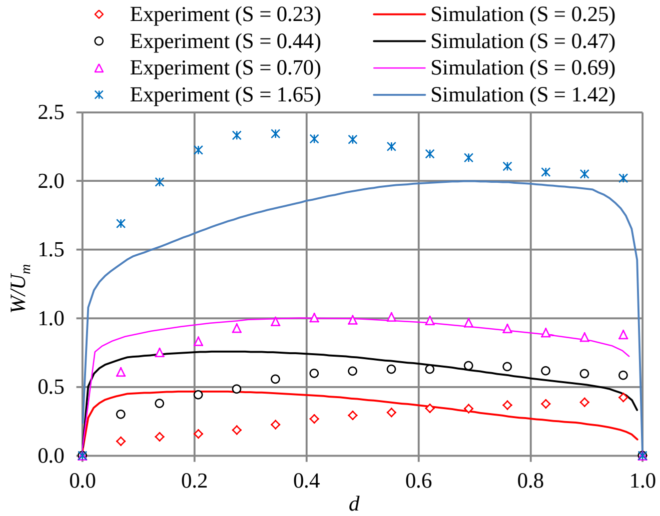

Figure 11. Normalised tangential velocity: comparison between experiment and simulations for 63 g/s mass flow within the annulus.

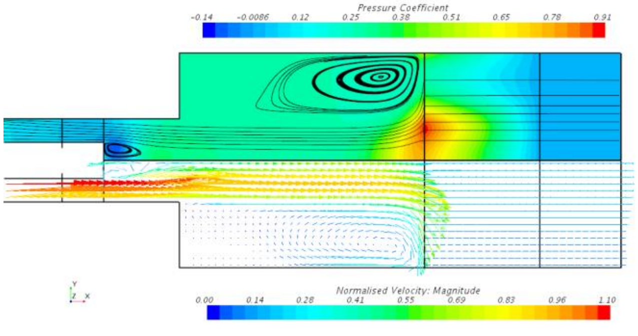

Figure 12. Pressure coefficient distribution, streamlines and normalised velocity vectors, $S = 0$. Velocity is normalised by mean inlet axial velocity.

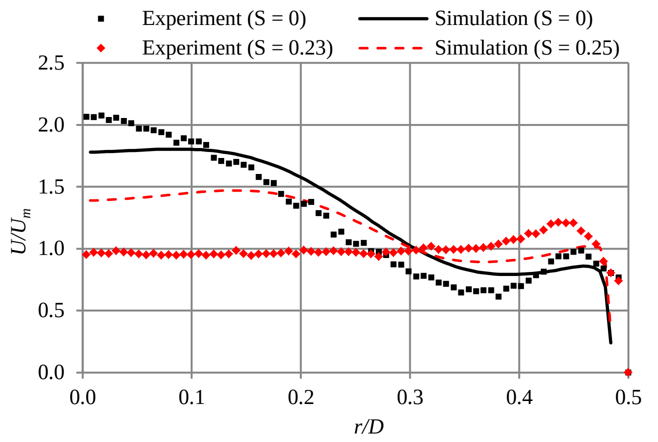

Figure 13. Velocity distribution 30 mm downstream of the monolith (normalised by the mean velocity in the same cross-section) for $S = 0$ and $S = 0.23$, 63 g/s.

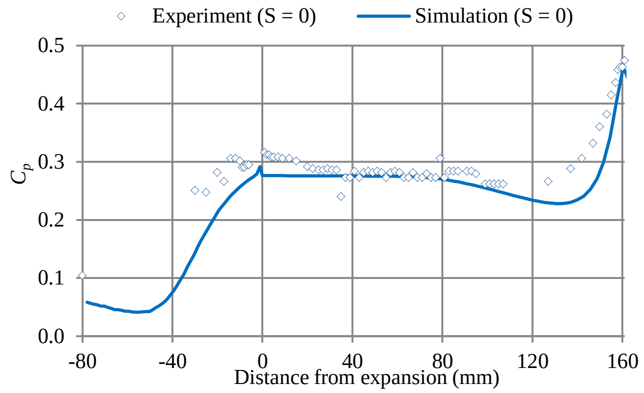

Figure 14. Pressure coefficient along the diffuser wall for $S = 0$, 63 g/s.

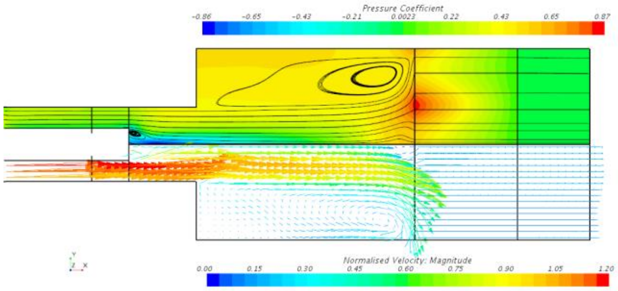

Figure 15. Pressure coefficient distribution, constrained streamlines and normalised velocity vectors, $S = 0.23$. Velocity is normalised by mean inlet axial velocity.

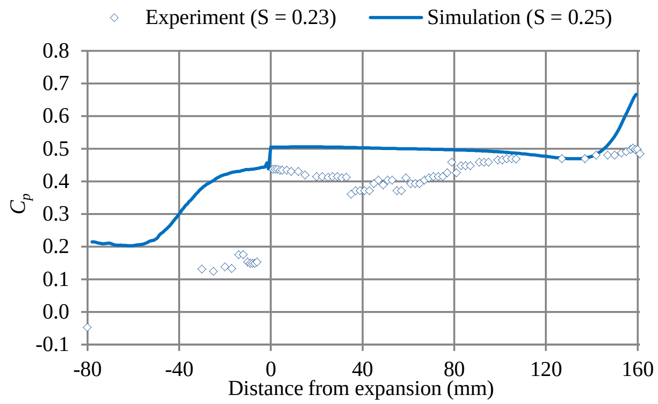

Figure 16. Pressure coefficient along the diffuser wall for S = 0.23, 63 g/s.

The flow downstream of the monolith (Figure 13) is mostly unidirectional with two velocity peaks: primary velocity peak in the middle and secondary velocity peak near the walls. The model underpredicts flow maldistribution in the monolith but captures the trend reasonably well.

Low swirl (S = 0.23)

Introduction of a swirling velocity component causes an increase in radial pressure gradients, and higher axial flow near the wall of the diffuser as a result (Figure 13). The trade-off between the inertia and centrifugal forces causes the nearly flat profile observed in the experiments, with slight peaks near the wall. The simulation correctly predicts the trend of the flow becoming more uniform with increasing swirl level, however it still shows a degree of non-uniformity throughout the cross-section. This may be caused by the slight underprediction of the inlet swirl levels as shown in Figure 11.

Figure 15 shows that the separation zone downstream of the sudden expansion still covers the whole diffuser wall. The pressure is noticeably lower along the diffuser axis, and the separation zone behind the annular insert becomes larger. The high pressure area at the monolith front face, where the jet slows down, has moved further towards the wall.

Pressure coefficient variation at the wall (Figure 16) also differs considerably between CFD and experimental results. Much better pressure recovery is observed in the experiment, without the steep gradient near the monolith front face.

Intermediate swirl (S = 0.44)

At swirl levels higher than 0.23, further increase of the separation zone size behind the annulus is predicted (Figure 17). In contrast, the separation zone at the sudden expansion shrinks considerably, and a pressure maximum at the wall marks the point of reattachment where the swirling jet reaches the wall (Figure 18). The general pressure distribution trend and the position of the reattachment point is predicted reasonably well, however CFD results exhibit much more pronounced pressure variation along the wall. In contrast to the low swirl case, the adverse pressure gradient on the centre line is capable of producing reverse flow.

Downstream of the catalyst, the velocity features a pronounced peak near the wall characteristic to swirling flows (Figure 19). Experimental and CFD results agree well, with CFD missing the "flat" part of the velocity profile around r/D = 0.25 and overpredicting the velocity magnitude in the centre.

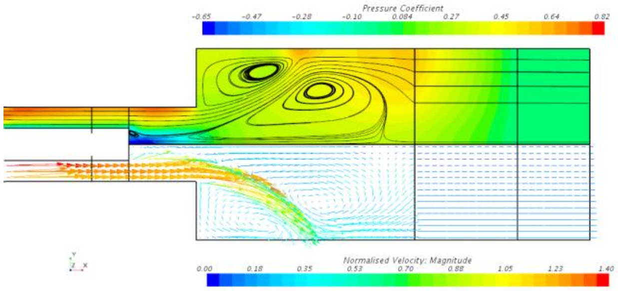

Figure 17. Pressure coefficient distribution, constrained streamlines and normalised velocity vectors, S = 0.44. Velocity is normalised by mean inlet axial velocity.

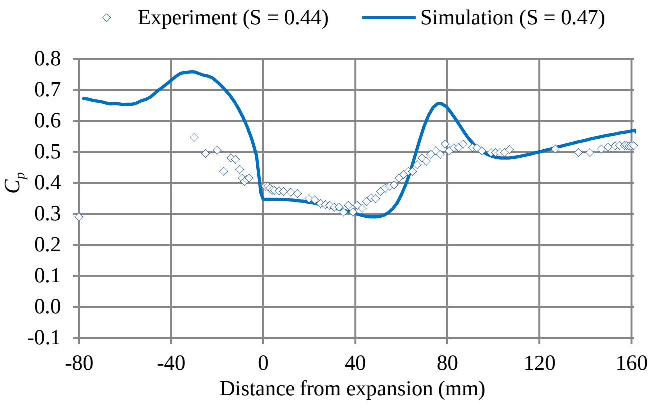

Figure 18. Pressure coefficient along the diffuser wall for S = 0.44, 63 g/s.

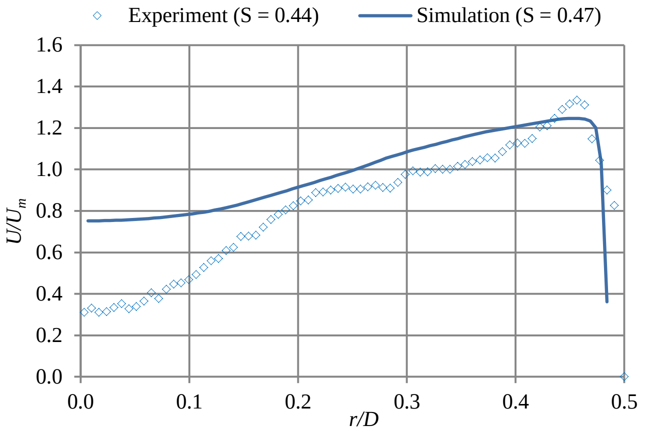

Figure 19. Velocity distribution 30 mm downstream of the monolith (normalised by the mean velocity in the same cross-section) for S = 0.44, 63 g/s.

Swirl levels (S = 0.70 and S = 1.65)

Increasing swirl further results in the adverse pressure gradients near the axis so high that the central recirculation zone now stretches all the way through the catalyst (Figure 20, Figure 21). It causes reverse flow near the axis of the monolith and further downstream. This is a well-known feature of highly swirling flows, when high radial pressure gradients induced by swirl result in adverse axial pressure gradients along the axis of the assembly.

Thus, the axial velocity downstream of the monolith features a maximum near the walls and reverse flow near the axis of the assembly (Figure 22, Figure 23). Comparison with experimental measurements shows a reasonable agreement with the hot wire velocity measurements. Simulations underpredict velocity variation, with velocity maxima and minima magnitudes lower than those observed in experiments for the highest swirl level. The apparent underprediction of the minimum velocity is due to the inability of HWA to detect reverse flow. Hot-wire anemometry only measures the magnitude of the velocity, thus the velocities are shown as positive where reverse flow is observed near the axis of the assembly.

The separation zones in the diffuser corners shrink further so that the (high-pressure) stagnation point where the jet meets the wall is shifted toward the corner (Figure 24, Figure 25). It is expected that at higher swirl levels the separation zones will disappear completely.

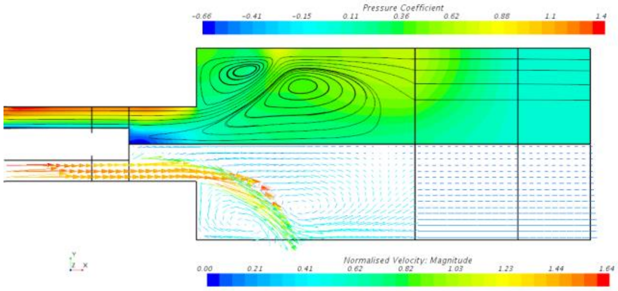

Figure 20. Pressure coefficient distribution, constrained streamlines and normalised velocity vectors, S = 0.7. Velocity is normalised by mean inlet axial velocity.

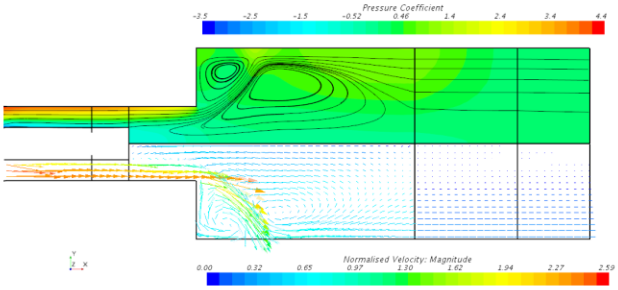

Figure 21. Pressure coefficient distribution, constrained streamlines and normalised velocity vectors, S = 1.65. Velocity is normalised by mean inlet axial velocity.

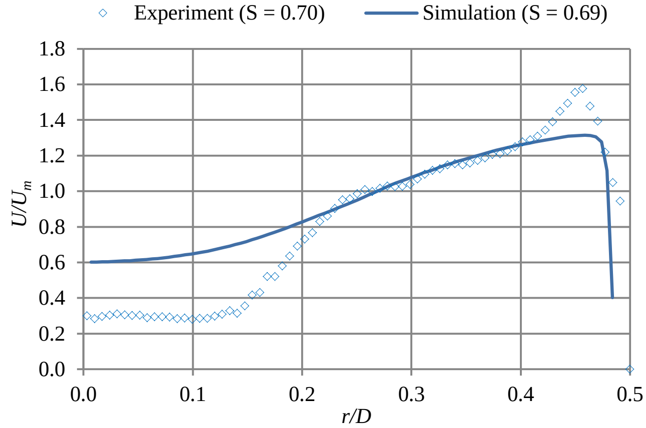

Figure 22. Velocity distribution 30 mm downstream of the monolith (normalised by the mean velocity in the same cross-section) for S = 0.70, 63 g/s.

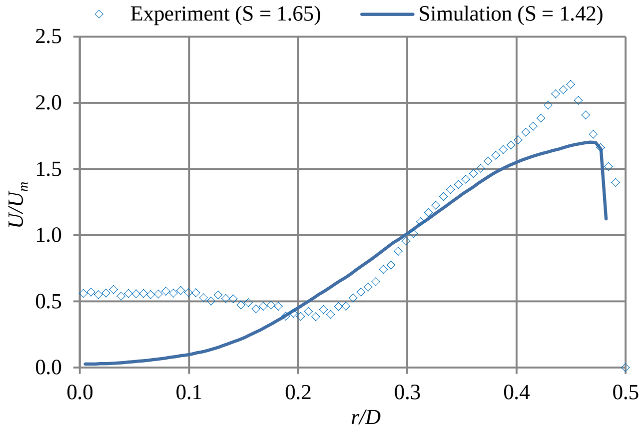

Figure 23. Velocity distribution 30 mm downstream of the monolith (normalised by the mean velocity in the same cross-section) for S = 1.65, 63 g/s.

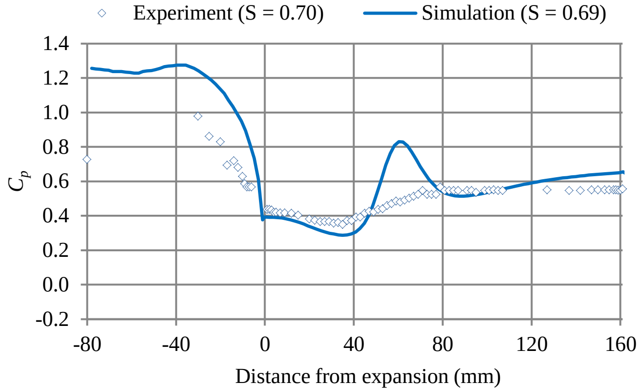

Figure 24. Pressure coefficient along the diffuser wall for S = 0.70, 63 g/s.

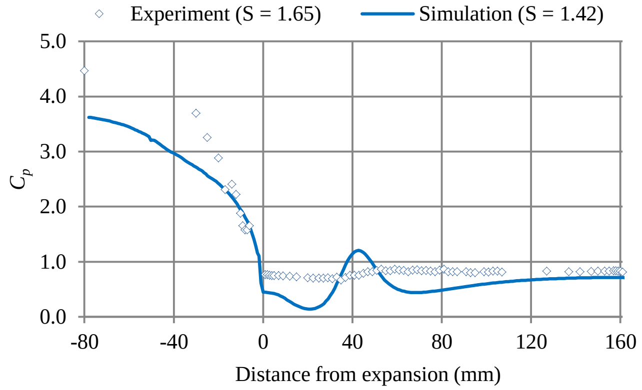

Figure 25. Pressure coefficient along the diffuser wall for S = 1.65, 63 g/s.

Conclusion

The effect of swirl on flow uniformity in a catalyst has been investigated experimentally and numerically. The results confirm that an optimal swirl level exists where the flow in the catalyst is most uniform with the maldistribution index of 0.4. This flow regime occurs when the inertial force driving the central jet in the diffuser is balanced by the centrifugal force forcing the flow to redistribute towards the diffuser wall. It happens for relatively low swirl levels (S ~ 0.23).

CFD simulations demonstrate that a simple RANS-based methodology is sufficient to get an insight into the main flow features and mechanisms governing flow redistribution depending on swirl. Velocity profiles downstream of the catalyst are predicted well, while pressure variation at the diffuser wall is generally overpredicted. The results also indicate that the most uniform flow regime is predicted to occur at higher swirl levels, compared to experiment.

In general, a RANS-based CFD model has predicted the most important flow features at lower and higher swirl levels reasonably well. However, the model fails to correctly predict the flow regime where the flow changes from a central jet dominated pattern to the wall jet dominated pattern. This is attributed to the fact that the flow distribution is very sensitive to the swirl levels upstream of the assembly, and these are not predicted with sufficient accuracy by RANS. Moreover, the delicate balance between the opposing forces dominating the central jet and the wall jet regimes in the diffuser is affected by the intrinsic anisotropy of the flow turbulence. Thus, the isotropic v^2f model is not suitable for exploring this flow regime. Using anisotropic turbulence models, such as a Reynolds Stress Turbulence model or the more complex Large Eddy Simulation models are needed for improving flow predictions. This is subject of ongoing work.

The findings can be used in the design of aftertreatment devices (e.g. catalysts and filters), where swirl levels could be adjusted by optimising the aftertreatment system geometry downstream of the turbocharger.

References

1. Martin, A. P., Will, N. S., Bordet, A., Cornet, P. et al., "Effect of Flow Distribution on Emissions Performance of Catalytic Converters," SAE Technical Paper 980936, 1998, doi: 10.4271/980936.

2. Wendland, D. W., Sorrell, P. L. and Kreucher, J. E., "Sources of Monolith Catalytic Converter Pressure Loss," SAE Technical Paper 912372, 1991, doi: 10.4271/912372.

3. So, K. L., "Vortex Phenomena in a Conical Diffuser," *AIAA J.* 5(6):1062-1078, 1967, doi: 10.2514/3.4139.

4. Clausen, P. D., Koh, S. G. and Wood, D. H., "Measurements of a Swirling Turbulent Boundary Layer Developing in a Conical Diffuser," *Exp Therm Fluid Sci.* 6(1):39-48, 1993, doi: 10.1016/0894-1777(93)90039-L.

5. Okhio, C. B., Horton, H. P. and Langer, G., "Effects of Swirl on Flow Separation and Performance of Wide Angle Diffusers," *Int J Heat Fluid Fl*. 4(4):199-206, 1983, doi: 10.1016/0142-727X(83)90039-5.

6. McDonald, A. T., Fox, R. W. and Van Dewoestine, R. V., "Effects of Swirling Inlet Flow on Pressure Recovery in Conical Diffusers," *AIAA J*. 9(10):2014-2018, 1971, doi: 10.2514/3.6456.

7. Senoo, Y., Kawaguchi, N. and Nagata, T., "Swirl Flow in Conical Diffusers," *B JSME*. 21(151):112-119, 1978, doi: 10.1299/jsme1958.21.112.

8. Ramji, S. A., Tarun, M., Bharath, R., Arumugam, A. S., et al., "A Parametric Study on the Improvement of Pressure Recovery Coefficient of a Conical Diffuser using Computation Fluid Dynamics," in *2013 International Conference on Energy Efficient Technologies for Sustainability (ICEETS)*, Nagercoil, 2013, doi: 10.1109/ICEETS.2013.6533388.

9. Escudier, M. P. and Keller, J. J., "Recirculation in Swirling Flow: A Manifestation of Vortex Breakdown," *AIAA J*. 23(1):111-116, 1985, doi: 10.2514/3.8878.

10. Dellenback, P. A., Metzger, D. E. and Neitzel, G. P., "Measurements in Turbulent Swirling Flow through an Abrupt Axisymmetric Expansion," *AIAA J*. 26(6):669-681, 1988, doi: 10.2514/3.9952.

11. Escudier, M. P., Bornstein, J. and Zehnder, N., "Observations and LDA Measurements of Confined Turbulent Vortex Flow," *J Fluid Mech*. 98(1):49-63, 1980, doi: 10.1017/S0022112080000031.

12. Leuckel, W., "Swirl Intensities, Swirl Types and Energy Losses of Different Swirl Generating Devices," *IFRF Doc No. G02/a/16*, 1967.

13. Skusiewicz, P., "*Effect of Swirl on the Flow Distribution across Automotive Emissions After-treatment Devices"*, M.Sc. thesis, Coventry University, 2012.

14. Wendland, D. W. and Matthes, W. R., "Visualization of Automotive Catalytic Converter Internal Flows," SAE Technical Paper 861554, 1986, doi: 10.4271/861554.

15. Ramadan, B. H., Lundberg, P. C. and Richmond, R. P., "Characterization of a Catalytic Converter Internal Flow," SAE Technical Paper 2007-01-4024, 2007, doi: 10.4271/2007-01-4024.

16. Munnannur, A., Cremeens, C. M. and Gerald Liu, Z., "Development of Flow Uniformity Indices forPerformance Evaluation of Aftertreatment Systems," *SAE Int. J. Engines*. 4(1), 2011, doi: 10.4271/2011-01-1239.

17. Wegner, B., Maltsev, A., Schneider, C., Sadiki, A., et al., "Assessment of unsteady RANS in predicting swirl flow instability based on LES and Experiments," *Int. J. Heat Fluid Fl*. 25(3):528–536, 2004, doi:. 10.1016/j.ijheatfluidflow.2004.02.019.

18. Iaccarino, G., "Predictions of a Turbulent Separated Flow Using Commercial CFD Codes," *J. Fluids Eng*. 123(4):819-828, 2001, doi: 10.1115/1.1400749.

19. Benjamin, S. F. and Roberts, C., "Three-dimensional modelling of NOx and particulate traps using CFD: A porous medium approach," *Appl Math Model*. 31(11):2446-2460, 2007, doi: 10.1016/j.apm.2006.10.015.

20. Quadri, S. S., Benjamin, S. F. and Roberts, C., "An Experimental Investigation of Oblique Entry Pressure Losses in Automotive Catalytic Converters," *P I Mech Eng C-J Mec*, 223(11): 2561-2569, 2009, doi: 10.1243/09544062JMES1565.

Contact Information

ruslii@uni.coventry.ac.uk

s.aleksandrova@coventry.ac.uk

Acknowledgments

We would like to acknowledge the support of our colleagues Jonathan Saul, Lawrance King, Dr. Carol Roberts and Piotr Skusiewicz.

Definitions/Abbreviations

CFD	Computational fluid dynamics
DOC	Diesel oxidation catalyst
GUI	Graphical user interface
HWA	Hot-wire anemometry
RANS	Reynolds-averaged Navier-Stokes
SN	Single-normal

Reply to reviewers

We would like to thank all reviewers for their constructive comments that helped improve the paper quality. In addition to the revisions listed below in response to the reviewers, a few minor amendments have been made to the paper. The abstract was slightly expanded to add some application context for more general readers (two sentences added at the beginning of the abstract and three sentences at the end) and figure legends have been amended for consistency.

Reviewer 1

The paper is well written and requires only minor editorial modification prior to publication:

(a) The **variables in equations (2) and (3) are not clearly defined in the text**, as was done for equation (6). This should be added for clarity.

The variables in equations (2) and (3) have been added in the text on page 3 with supporting clarification provided by Figure 3.

(b) A brief discussion would be useful as to **why the simulated swirl number for the 10 degree swirl angle is significantly different than the experimental values (relative to other angles) (Table 1)**

We would like to thank the reviewer for pointing this out. The value in the table was a misprint. The correct value for simulations is 0.69 for 10 degree diffuser, which is in reasonable agreement with the experimental values. It has now been corrected.

(c) On page 5, in the left column in the 3rd from last paragraph, **the word "the" should be included before "SIMPLE"**

The word "the" has been added before the word "SIMPLE" on page 5, in the right column in the 4th from last paragraph.

Reviewer 2

Manuscript 17FFL-0049 "The Effect of Swirl on the Flow Uniformity in Automotive Exhaust Catalysts" presents a combined experimental and numerical study on an aftertreatment (AT) system that experiences flow with various levels of swirl. The topic is of relevance to AT community, and findings are applicable particularly for close-coupled systems. This work will be a welcome addition to AT literature, and **it would have been interesting to compare the experimental data with simulations done using an anisotropic turbulence model** , since it is well known that isotropic models have inadequancies in capturing swirling flows. This manuscript could be accepted if the authors address the following comments through revisions to their manuscript or a well-reasoned rebuttal.

We agree with the reviewer that anisotropy plays a major role in swirling flows. As mentioned in the Conclusions, work is currently in progress to assess the potential of anisotropic RANS models (such as Reynolds Stress Model) and more complex models such as Detached Eddy Simulations and Large Eddy Simulations. This initial CFD study was performed to aid in the interpretation of the experimental data but also served to provide an assessment of the limitations of the isotropic models which are still the most feasible option for the industrial applications.

Major comments:

- Table 1 : For intermediate and high swirl, the Swirl numbers used in simulations differ relatively more from those measured in tests. **Is this due to inadequate representation of flow features in geometry or experimental and numerical uncertainties? Why did not the authors attempt to match the measured swirl numbers ?**

Q1 – We would like to thank the reviewer for pointing this out. One value in the table was misprinted. The correct value for simulations is 0.69 for 10 degree swirl generator angle, which is in reasonable agreement with the experimental values. It has now been corrected. For high swirl (18 degree swirl generator angle), the difference in the swirl numbers is indeed caused by the underprediction of swirl levels in the simulations.

Q2 – The predicted swirl level immediately upstream of the test section is not controlled directly and is the result of simulating the flow inside the swirl generator with the appropriate swirl generator angle. Therefore, it is difficult to match the swirl number exactly. However, another experimental/numerical study is ongoing which will demonstrate in detail how the flow and the swirl levels change with the swirl generator angle setting, and we are expecting to be able to match the swirl numbers and compare results between the experiments and the CFD predictions.

- Page 6 : authors state that "..The offset of pressure might be attributed to the prescription of the losses in the monolith." **What does this mean ? How were the inertial and viscous coefficients derived (e.g., from cold flow tests)? How did the authors check if these coefficients are indeed correct for the catalyst used?**

Q1 – The offset was caused by the fact that the porous and inertial resistance coefficients (page 5, column 2, paragraph 3) were estimated from the best fit line from the experimental data for a wide range of mass flow rates. Unfortunately, for lower superficial velocities used here the best fit line did not match the experimental data very well. To rectify this problem, we have now amended the best fit line to match the lower mass flow rate range better, and rerun the simulations. The pressure coefficients now agree with the experimental values much better. Other flow variables changed slightly too, and all corresponding figures have been amended (Figures 10 - 25).

Q2 – The resistance coefficients have been obtained from cold flow tests. This is now clarified on Page 5, column 2, second paragraph from last.

Q3 – The resistance coefficient testing in [13] has been performed on the same catalyst brick used for this study, and therefore should describe the resistance adequately. It has now been clarified in the text (Page 5, column 2, end of second to last paragraph).

- **How was channel flow enforced in simulations? How high were the resistances used in non-axial directions compared to those used in axial (along the main flow) direction?**

Q1 – The porous medium approach does not separate the flow into individual channels [19]. However, very high resistance values are used in the non-axial directions to ensure the flow is unidirectional. This approach has been used in many previous studies and has been shown to work well (see e.g. Porter, S., Saul, J., Aleksandrova, S., Medina, H. & Benjamin, S. (2016) Applied Mathematical Modelling 40, p. 8435-8445).

Q2 – The resistances (both viscous and inertial) in the directions tangential to the flow were set to 10^5, i.e. 3 orders of magnitude higher than that in the axial direction. Higher resistances cause convergence problems, however it has been checked that the flow in the porous region is essentially one-directional.

Minor comments:

- Definitions of variables used in various equations have not been provided. Please add them.

Eqns. (1) to (3) – definitions of the variables ρ, U, W, r, r_o and r_i have been added and are complemented by Figure 3.

Eqn. (4) – definitions of the variables peak velocity and mean velocity have been added in the text on page 5

Eqn. (5) – definitions have been included in the text on page 5

Resistance coefficients (page 5) – definitions have been included in the text on page 5

$\Delta p_{oblique} = \pm\rho v^2/2$ – definition of ρ has been added in the text on page 5

Eqn. (6) – definitions have been included on page 6

- Ref .13 does not include sufficient details on the referenced publication . Is this a thesis or an internal report?

Ref. 13 is a Master of Science thesis, the details of which have been updated in the References section